Oxygen Activation in Aromatic Ring Cleaving Salicylate Dioxygenase: Detection of Reaction Intermediates with a Nitro-substituted Substrate Analog

Qian Wang[‡], Hanbin Li[‡,§], Uran Bujupi[‡], Janosch Gröning[†], Andreas Stolz[†], Angelo Bongiorno[‡,§,*] and, Rupal Gupta[‡,⊥,§,*]

[‡]*Department of Chemistry, College of Staten Island, The City University of New York, 2800 Victory Blvd. Staten Island, New York, 10314, United States*
[†]*Institut für Mikrobiologie, Universität Stuttgart, Allmandring 31, 70569 Stuttgart, Germany*
[⊥]*Ph.D. Programs in Biochemistry, The Graduate Center of the City University of New York, United States*
[§]*Ph.D. Programs in Chemistry and Physics, The Graduate Center of the City University of New York, United States*

***Corresponding authors:** Rupal Gupta, Department of Chemistry and Biochemistry, College of Staten Island, The City University of New York, USA, Tel: (718) 982-3936; Email: rupal.gupta@csi.cuny.edu
Angelo Bongiorno, Department of Chemistry and Biochemistry, College of Staten Island, The City University of New York, USA, Tel: (718) 982-3926; Email: angelo.bongiorno@csi.cuny.edu

Abstract

Cupin dioxygenases such as salicylate 1,2-dioxygense (SDO) perform aromatic C-C bond scission via a 3-His motif tethered iron cofactor. Here, transient kinetics measurements are used to monitor the catalytic cycle of SDO by using a nitro-substituted substrate analog, 3-nitrogentisate. Compared to the natural substrate, the nitro group reduces the enzymatic k_{cat} by 500-fold, thereby facilitating the detection and kinetic characterization of reaction intermediates. Sums and products of reciprocal relaxation times derived from kinetic measurements were found to be linearly dependent on O_2 concentration, suggesting reversible formation of two distinct intermediates. Dioxygen binding to the metal cofactor takes place with a forward rate of 5.9×10^3 $M^{-1}s^{-1}$: two orders of magnitude slower than other comparable ring-cleaving dioxygenses. Optical chromophore of the first intermediate is distinct from the *in situ* generated SDO Fe(III)-$O_2^{\bullet-}$ complex but closer to the enzyme-substrate precursor.

Introduction

Metalloenzymes catalyze energetically challenging reactions with the aid of their metal cofactors. Dioxygenases are a broad class of enzymes that incorporate both atoms of dioxygen into their organic substrates during biotransformations. Catalysis performed by ring cleaving dioxygenases is of interest not only due to their fundamental role in carbon recycling but also because of possible applications in degradation of environmental pollutants such as polychlorinated biphenyls.[1] Gentisate 1,2-dioxygenase (GDO) is a cupin dioxygenase, which performs aerobic degradation of its dihydroxylated substrates such as gentisate by cleaving the aromatic C-C bond.[2-4] Cupin superfamily of proteins bear a structurally distinct conserved β-barrel fold.[5] Cupin proteins, including dioxygenases, are one of the most functionally diverse family of proteins; members of this family transform a broader range of aromatic substrates. While several cupin dioxygenases have been structurally characterized (*vide infra*), their catalytic mechanism has not been investigated.

Members of the GDO family are homotetrameric proteins with each monomer containing a Fe cofactor ligated to the protein derived 3-His binding motif. First identified in *Pseudaminobacter salicylatoxidans* BN12, salicylate 1,2-dioxygenase (SDO) is a unique member of the GDO family.[6] Albeit bearing 70% sequence similarity to GDO, SDO exhibits remarkable substrate promiscuity by transforming monohydroxylated substrates such as salicylate in addition to gentisate (Scheme 1).[7-10] More recently, SDO from bacterium *Pseudaminobacter salicylatoxidans* DSM 6986^T has also been shown to exhibit amidohydrolase activity by transforming mycotoxin ochratoxin A.[11]

Scheme 1. Reaction catalyzed by GDO (R_3 = OH) and SDO (R_3 = H or OH).

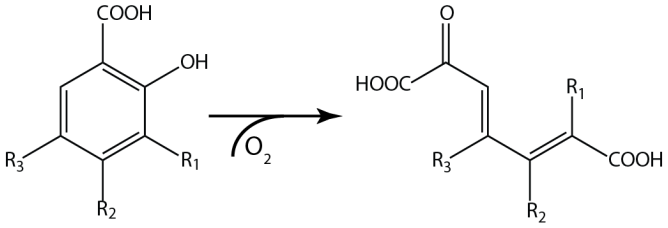

SDO is the most structurally characterized enzyme within the GDO family with several reported crystal structures of the wild type and mutant protein in the presence and absence of substrates.[7, 12-13] These studies have demonstrated that gentisate binds to the Fe center via a bidentate binding mode. Biochemical and spectroscopic studies reveal that in its active state, iron cofactor assumes a +2 oxidation.[3, 14] Several key active site residues assist in SDO catalysis. For instance, mutagenesis studies show that His162 and Arg127 are critical for catalysis; substituting these residues with other amino acids either significantly diminishes or entirely eradicates the enzyme activity.[15] Additionally, previous biochemical studies have also proposed that these residues may undertake the roles of acid/base and participate in catalysis. However, quantum mechanics and molecular mechanics (QM/MM) studies showing that Arg127 forms hydrogen

bonds with bound dioxygen molecule, have disputed this hypothesis suggesting a lack of proton source during O_2 activation, and therefore raising the possibility that SDO undergoes an atypical O_2 activation pathway.[16]

Mechanisms of O_2 activation and subsequent chemical transformations by nonheme enzymes have captured the widespread interest of scientific community. Due to the short lifetimes of the reaction intermediates, detection of all transient species and their detailed electronic and kinetic characterization remains a challenge. Widely accepted reaction scheme for aromatic ring cleaving (ferrous) dioxygenases entails formation of an oxy intermediate upon O_2 binding to the enzyme-substrate complex (ES). Formation of this oxy intermediate is the first step in O_2 activation. Based on spectroscopic and computation studies, this intermediate is assumed to bear a ferric-superoxide electronic configuration.[17-19] However, such species have only been experimentally observed in a handful of enzymes impeding the development of a clear mechanistic pathway for non-heme dioxygenases.[18, 20-21] The proposed reaction mechanism for GDO and SDO involves the formation of a semiquinone radical coupled to a Fe(II)-superoxide species upon formation of the oxy complex.[22] The two radicals around the metal cofactor recombine to yield a bridged alkylperoxo intermediate upon which, the reaction proceeds by insertion of oxygen atoms into the substrate (Scheme 2). Given that no reaction intermediates have been experimentally detected, their electronic properties and the reaction mechanism remains ambiguous. For instance, what is the nature of the oxy intermediate in SDO? How does such an intermediate compare with its counterparts from other ring cleaving iron dioxygenases? This work aims to address these open questions.

Scheme 2. Proposed reaction mechanism of SDO (R = OH for gentisate and H for salicylate)

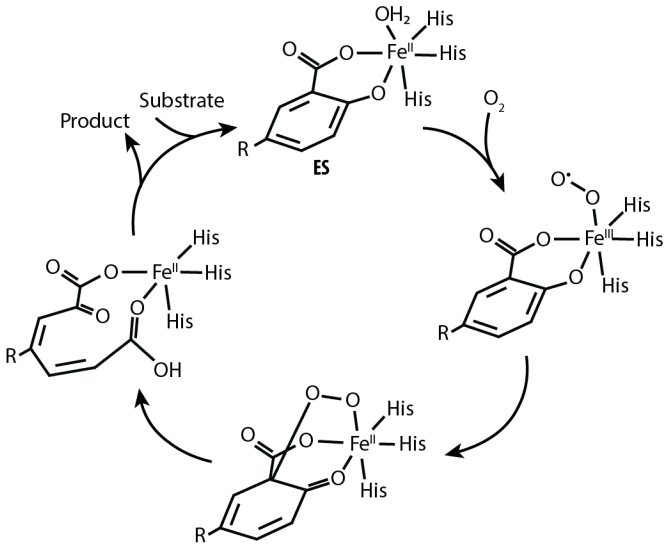

In addition to the central quest of clarifying the reaction mechanisms of dioxygenases, SDO poses several key questions regarding the architecture of the active sites in this class of enzymes with a focus towards our general understanding of biological catalysis. In contrast to other ring cleaving dioxygenases with canonical 2-His-1-Carboxylate binding motif,[23-24] iron cofactor in SDO is tethered to three histidine residues yielding an additional positive charge to the metal-ligand catalytic center. In addition to this, the active site of SDO is composed of several positively charged amino acids (H162, Arg127, Arg83) that participate in secondary sphere interactions. While variations in the primary coordination sphere in the context of the overall charge of the metal-ligand complex may dictate the substrate binding mode and/or its ionic form to execute charge maintenance,[25-26] such large positive charge may also influence the reaction coordinates by altering the reaction pathway, its energetics or kinetics. Therefore, evaluating these factors in the context of other atypical coordination motifs such as 3-His-1-Carboxylate[27] and 4-His[28] will not only provide a deeper mechanistic insight, but may also enable the design of complex artificial metalloenzymes with customizable parameterization of primary and secondary sphere to achieve desired reaction outcomes.

Several strategies have been utilized to capture transient reaction intermediates in enzymatic cycles including enzyme variants and the use of alternate substrates that can attenuate the rection kinetics.[18, 29-31] For ring cleaving dioxygenases, incorporation of electron withdrawing groups into the aromatic substrate affords sluggish enzymatic activity and offers an opportunity to monitor the reaction pathway. In particular, Lipscomb and coworkers demonstrated that nitro substituted substrate analogs not only attenuate enzyme activity but also facilitate detailed characterization of the reaction cycle by introducing distinct optical chromophores for the substrate and product.[18, 29, 32] In this report, we use this strategy to evaluate the reaction cycle of SDO by incorporating a nitro group to its natural substrate, gentisate. Using nitro substituted gentisate as a substrate analog and stopped-flow optical absorption spectroscopy, we report detection of two reaction intermediates of SDO. Kinetic parameters derived from transient kinetics measurements provide insights into SDO catalytic cycles and allows for a direct comparison with other similar iron dioxygenases.

Results

Reaction of 3-nitrogentisate with SDO. The absorption maximum of 3-nitrogentisate (3NG) in solution at pH 8.0 changes from 390 nm to 345 nm upon reaction with SDO (Figure S1). ^{1}H NMR studies of the product of the reaction dissolved in D_2O showed two singlets at 7.79 and 7.08 ppm, consistent with the substrate undergoing a bond scission between carbon 1 and carbon 2 of the aromatic ring. The observed bond cleavage is consistent with the ring scission in the natural product, gentisate, suggesting that incorporation of the nitro group does not alter the primary reaction catalyzed by the enzyme. Steady state kinetic parameters for the reaction of SDO with gentisate and 3NG are presented in Table 1. In aromatic

ring degrading oxygenases, electron withdrawing groups have been demonstrated to impair the transfer of electrons from the substrate to the metal center, thereby attenuating the overall reaction kinetics.[29] Consistent with the previous reports in the literature, incorporation of the nitro group attenuates the turnover number by approximately 500-fold compared to gentisate while the Michaelis-Menten constant remains relatively unchanged.

Table 1. Steady state kinetics parameters for the reaction of SDO with gentisate and 3NG at 4 ºC.

	K_m [µM]	k_{cat} [s^{-1}]
gentisate	198	154
3-nitro gentisate	183	0.3

Ionization state of enzyme bound 3NG (SDO-3NG). The optical spectrum of 3NG is highly sensitive to its ionization state. Previous studies in the literature have demonstrated that ligation to the ferrous center does not perturb the optical chromophore originating from the aromatic substrate.[15, 30] Therefore, the absorption maximum (λ_{max}) of 3NG can be used as a probe to identify its protonation state upon binding to the enzyme. pH titration of 3NG alone dissolved in water indicates two clear inflection points. A λ_{max} of 390 nm is observed between pH 4.0 to 8.5, indicative of its monoanionic state with a deprotonated carboxylate group. As the pH is increased from 8.5 to 10.5, the λ_{max} gradually shifts from 390 to 440 nm, suggestive of a dianionic state. This ionization state could originate from deprotonation of the hydroxyl group at position 2 or 5 in the aromatic ring. At pH values around 12, a λ_{max} of 550 nm is observed from the tri-anionic state of the compound. Anaerobic SDO-3NG complex (see below) at pH 8.0 exhibits a λ_{max} at 430 nm. In contrast to its free form in solution (pH 8.0) where both OH groups remain protonated, λ_{max} at 430 nm suggests that upon binding, 3NG undergoes a large shift in one of its ionization constants and ligates to the iron cofactor in predominantly dianionic form. Previous studies have indicated that the hydroxyl group of salicylate is deprotonated upon binding to SDO.[15] Taken together, these results indicate that 3NG binds to SDO in its dianionic form with the hydroxyl group at position 2 deprotonated. Additionally, the incorporation of the nitro substituent does not appear to influence the protonation state of the bound substrate.

Single turnover of SDO-3NG complex with O_2. In order to monitor SDO catalyzed reaction of O_2 and 3NG, anaerobic SDO-3NG complex was rapidly mixed at 4 ºC with solutions containing different O_2 concentrations. The reaction profile can be separated into three segments for clarity. During the first 0.5 seconds of the reaction, diode array traces of stopped-flow optical absorption spectroscopy (SF-Abs) show a decrease in the absorbance of the SDO-3NG complex at 430 nm, a shift in the λ_{max} to 420 nm and an isosbestic point at 348 nm, indicative of formation of an intermediate (Figure 1A). As the reaction progresses, in the timeframe of 0.5-1.5 s, the 420 nm absorbance continues to drop with very subtle increase in absorbance at 340 nm and the isosbestic point shifts to 356 nm. This may suggest formation of a second

intermediate with smaller extinction coefficient and λ_{max} near 340 nm (Figure 1B). In the last phase of the reaction between 1.5-6s, the isosbestic point further moves to 370 nm. However, during this timeframe large increase in the absorbance near 340 nm is observed with λ_{max} at 345 nm (Figure 1C). This absorption maximum of 345 nm represents the product formation. The shift in the isosbestic point and significant increase in absorbance corresponding to λ_{max} of 345 nm indicates that this phase of the reaction is distinct from the previous phase during 0.5-1.5 s. Another representation showing change in the absorbance between 0.01 and 6 s is presented in Figure S1 (right panel) demonstrating that no additional optical chromophores are observed during the time course of the reaction.

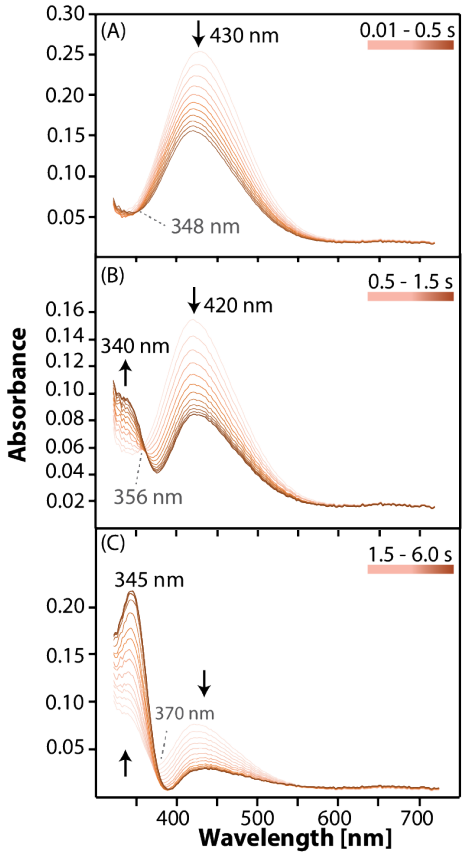

Figure 1. SF-Abs kinetics of the reaction of 100 µM SDO-3NG with 920 µM O_2 at 4 ºC and pH 8.0. The whole reaction is separated and displayed in three time segments: 0.01s-0.5 s (A); 0.5-1.5 s (B) and; 1.5-6.0s (C). Solid arrows represent λ_{max} that undergo increase or decrease during the course of the reaction and dashed gray lines represent the isosbestic points. Absorbance corresponding to enzyme was subtracted from all traces for clarity.

A more comprehensive analysis can be performed by determining reciprocal relaxation times (RRTs) using summed single exponentials fitted to the absorbance changes at various wavelengths during the time course of the reaction (see Experimental Methods). A representative SF-Abs trace at 367 nm for the reaction of 100 µM SDO-3NG complex with 920 µM O_2 at 4 ºC is shown in Figure 2. While a two exponential fit

can recapitulate the absorbance changes in the time range of 1-6s (Figure 2B), a third exponential is needed to accurately fit the initial phase of the reaction cycle (Figure 2C). Therefore, three exponentials are needed to best fit the entire time course of the reaction with RRTs of 8.0 ($1/\tau_1$), 0.84 ($1/\tau_2$) and 0.27 ($1/\tau_3$) s^{-1}. The first and second RRTs show clear dependence on O_2 concentration, while the third and the slowest phase remains relatively constant at various O_2 concentrations. Large differences in the magnitudes of $1/\tau_1$ and $1/\tau_2$ suggests that these RRTs depict two distinct steps in the reaction. Similarly, while $1/\tau_2$ and $1/\tau_3$ have similar magnitudes, their amplitudes have opposite sign, again indicating chemically distinct processes. Taken together, the three observed RRTs in our data denote three steps in the reaction cycle. Presumably, the first two RRTs represent reversible sequential steps in the reaction, preceding the ring opening. The magnitude of the last and the slowest step is similar to k_{cat} determined from steady state experiments (Table 1) and therefore should represent the rate determining irreversible product release step. These interpretations are in accordance with previous reported studies of non-heme iron dioxygenases.[32] Furthermore, the optical spectrum of the last step of the reaction is the same as that of the observed product in steady state measurements.

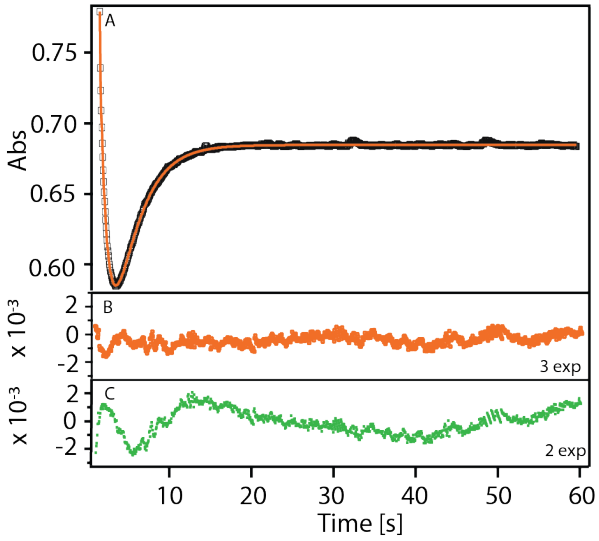

Figure 2. (A) Representative SF-Abs kinetics data at 367 nm showing the time course of the reaction of 100 μM Fe(II)-SDO-3NG complex with 920 μM O_2 at 4 ºC. The solid line represents three exponential fits to the data; (B) and (C) are the residuals to the trace using three and two exponentials, respectively.

Scheme 3. Reaction scheme for the observed intermediates in the catalytic cycles of SDO.

$$\text{SDO-NG+ } O_2 \underset{k_{-1}}{\overset{k_1}{\rightleftharpoons}} I_1 \underset{k_{-2}}{\overset{k_2}{\rightleftharpoons}} I_2 \xrightarrow{k_3} P$$

While the first RRT exhibits a clear dependence on O_2 concentration, $1/\tau_2$, representing the second phase of the reaction shows a non-linear O_2-dependence (Figure S2) suggesting that these two phases represent sequential steps in the reaction, instead of parallel pathways. Furthermore, nonlinear dependence of one phase of the reaction is indicative of reversible O_2 binding. Under this reaction scheme assuming two sequential reversible steps leading to the product formation (Scheme 3), concentration-time correlation of all the observable species in the reaction can be described by a series of differential equations. Experimentally observed RRTs are then defined by the roots of a cubic equation (see Supplementary Information) with the products and sums of the roots (or the RRTs) exhibiting a linear dependence on O_2 concentration. As shown in Figure 3, the sums and products of the experimentally derived RRTs yield the expected linear correlation with O_2 concentration. Therefore, the rates of the individual steps of the reaction can be extracted from the slopes and intercepts of RRT vs. O_2 concentration plots. Based on this analysis, the fastest step corresponding to the bimolecular process of O_2 binding has a forward rate constant (k_1) of $5.9 \pm 0.3 \times 10^3$ $M^{-1}s^{-1}$ and a backward rate (k_{-1}) of 2.0 ± 0.8 s^{-1}. This step results in the formation of the first observable intermediate in the reaction (herein referred as I1), which converts to the second intermediate (I2) at a forward rate, k_2 of 1.3 ± 0.14 s^{-1} and a reverse rate, k_{-2} of 0.24 ± 0.1 s^{-1}. Finally, the last step in the reaction corresponds to the conversion of I2 to the ring-opened product with a rate k_3 of 0.29 s^{-1}. The magnitude of k_3 is similar to k_{cat} determined from steady state experiments (Table 1) and consistent with the assumption that k_3 represents the last and the slowest step of the reaction.

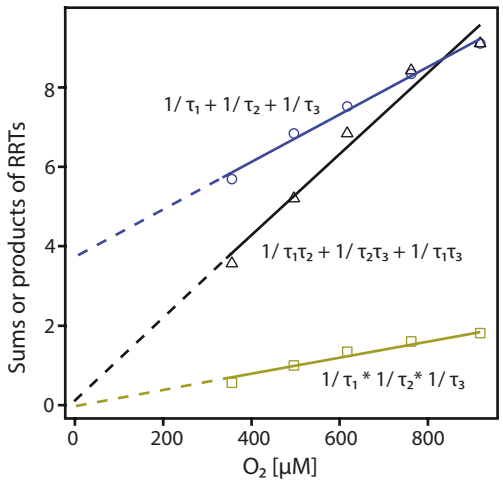

Figure 3. Plots of the sums and products of RRTs vs. the dissolved O_2 concentration with solid lines representing the best fits for a linear dependence.

Electronic structure of I1. Formation of I1 is the fastest probed step in the chemical reaction with the rate of formation (k_1) of 5.9×10^3 $M^{-1}s^{-1}$. The optical spectrum of I1 can be extracted based on the calculated rate constants of the reaction. The experimentally derived RRTs yield rate constants for the three observable steps based on Scheme 3, allowing for the determination of exact time-dependent concentrations of all

components of the reaction. The reaction coordinate describing the speciation profile vs time for the reaction of 100 μM Fe(II)-SDO-3NG with 920 μM O_2 at 4 ºC is shown in Figure S3. The first 20 ms of the reaction entail a linear decrease in the concentration of the ES complex with a concomitant increase in I1. During this timeframe, negligible amounts of I2 and product are formed. Additionally, the first diode array trace at 3 ms, which accounts for 98.6% enzyme substrate complex, can be approximated to represent the SDO-NG complex. Therefore, a subtraction of the diode array spectra at various timepoints within the first 18 ms accounting for appropriate proportions corresponding to the expected concentrations of the SDO-3NG yields the optical spectrum of I1. A comparison of the derived optical spectra of I1 (λ_{max} = 404 nm) as described above and SDO-3NG is shown in Figure 4.

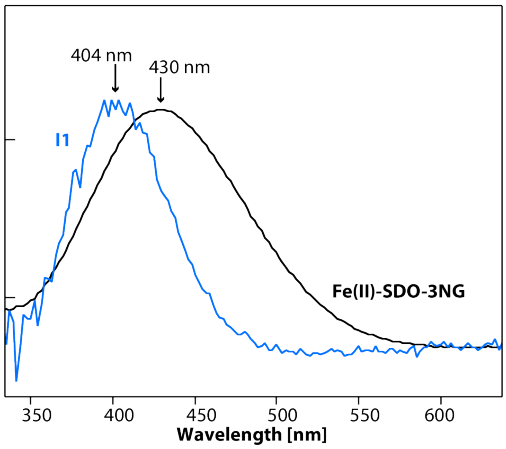

Figure 4. A comparison of optical chromophores of the Fe(II)-SDO-3NG complex (black) and I1 (blue). The optical spectrum of I1 was generated by the subtraction of diode array spectra collected within the first 20 ms of reaction initiation. Note that the absorbances (y-axis) of the two spectra have been arbitrarily scaled to match for clarity.

The enzyme bound dianionic form of the substrate exhibits a λ_{max} of 430 nm. A small blue shift in the absorption maximum of I1 compared to the bound dianionic substrate suggests that the substrate aromaticity is preserved. Being the first intermediate in the reaction cycle, it is likely that I1 is the SDO oxy adduct, Fe(II)-3NG-O_2. Such an intermediate, formed immediately upon the O_2 binding to the SDO-3NG complex, would be expected to retain the substrate aromaticity. This assignment is consistent with the findings of previously reported QM/MM calculations on SDO, which suggested that upon O_2 binding the planarity of the substrate is preserved in the salicylate-Fe(II)-O_2 complex, and the substrate is activated by partial transfer of electron density to O_2.[16] Such a transfer of electron density will also result in depletion of charge density from the substrate, giving rise to the observed shift in the optical spectrum reported here. Reaction cycles of non-heme iron dioxygenases are believed to be initiated upon binding of dioxygen to the ferrous center from partial transfer of the electron density from Fe center to the dioxygen moiety, yielding a formally Fe(III)-superoxo moiety. Therefore, the proposed oxy adduct of SDO, I1, *could* adopt an Fe(III)-

superoxo electronic configuration. To test this hypothesis we generated the superoxide complex of Fe(III)-SDO-3NG *in situ*.

Fe(III)-SDO was generated as described in *Supplementary Information*. As expected, Fe(III)-SDO exhibited no activity for the reaction with gentisate or 3NG with no detectable change in electronic absorption spectra of the substrates upon addition of the oxidized enzyme. Previous studies have demonstrated significant accumulation of superoxide anion in the xanthine oxidase (XO) catalyzed univalent reduction of O_2 under basic conditions.[21, 33-35] We utilized this approach to react Fe(III)-SDO with superoxide anions. Upon exposure of XO-generated superoxide anion to Fe(III)-SDO-3NG and Fe(III)-SDO-gentisate complexes, formation of the corresponding products was observed (Figure S4). Product formation was not observed when 3NG or gentisate were mixed with superoxide anion in the absence of the oxidized enzyme. Additionally, exposure of superoxide to Fe(III)-SDO in the absence of substrate did not generate the ferrous enzyme. These results indicates that superoxide anion can reactivate the oxidized enzyme to yield the product thereby acting as a chemical trigger. Thus, such a chemical rescue of the deactivated enzyme must take place upon binding of superoxide to the substrate bound ferric center leading to the formation of a Fe(III)-superoxo complex (Scheme 4).

Scheme 4. Overview of the observed and proposed intermediates in the reaction of SDO with 3NG. The colored double arrow alludes the equivalency between the oxy adduct and the Fe(III)-superoxo complex.

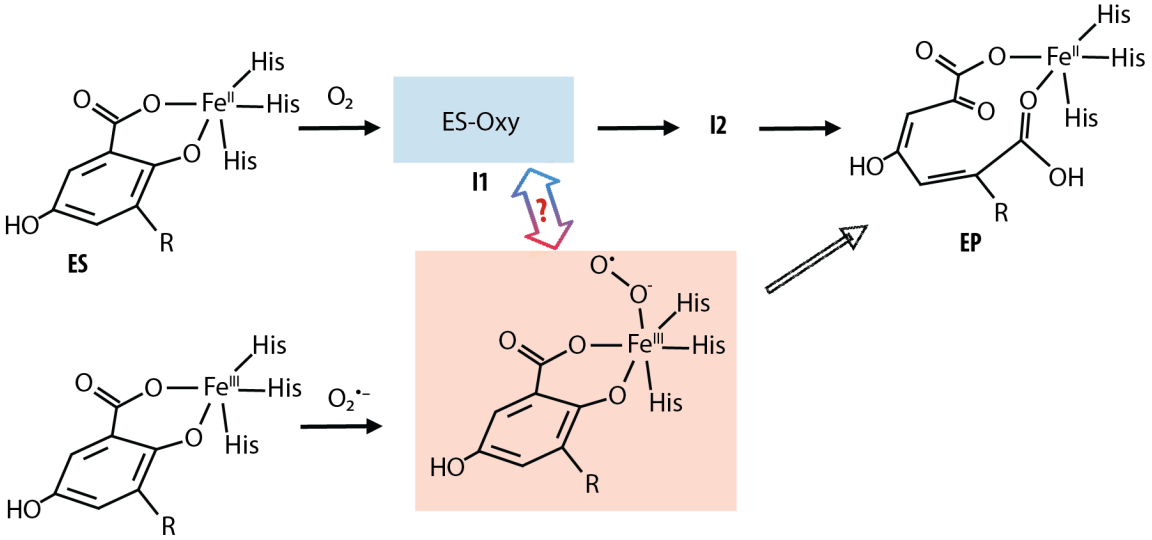

Generation of Fe(III)-SDO-3NG-superoxo complex. To detect the Fe(III)-superoxo complex formed upon binding of superoxide anion to the oxidized enzyme, we employed SF-Abs spectroscopy. Equimolar (100 μM) amounts of Fe(III)-SDO and 3NG were mixed under aerobic conditions to generate substrate bound ferric enzyme (Fe(III)-SDO-3NG). This complex was rapidly mixed with XO-generated $O_2^{\bullet-}$. Immediately

after the addition of $O_2^{\bullet-}$, rapid decrease in the absorbance in 450-550 nm region of the spectrum was observed (Figure 5A). This decrease was accompanied by subsequent increase in the absorbance at 345 nm corresponding to the product formation (Figure S4). A series of difference spectra generated upon subtracting the initial diode array spectrum at 0.018 s shows an optical feature centered at 495 nm (Figure 5B). As the reaction progresses, the species corresponding to this optical chromophore is consumed and the product is formed. The decay kinetics of this species leading to the product formation is complicated and not the focus of the current work. However, this species generated immediately upon rapid mixing of the substrate bound ferric enzyme and superoxide is presumably the Fe(III)-SDO-3NG-$O_2^{\bullet-}$ complex. The chromophore at 495 nm is also consistent with other Fe(III)-superoxide species reported in the literature (*vide infra*) and therefore, represents the 3NG bound ferric-superoxo complex of SDO. The time course of the reaction of Fe(II)-SDO-3NG with O_2 (Figure 1) showed no evidence for the formation of a species with λ_{max} at 495 nm. Differences in the optical spectra of I1 and chemically derived Fe(III)-SDO-3NG-$O_2^{\bullet-}$ complex suggests that these two species are not identical.

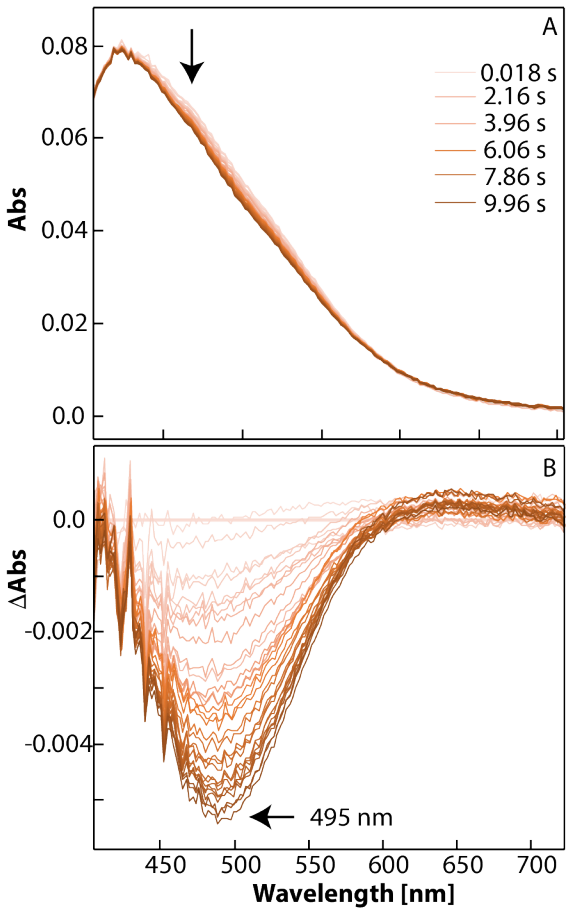

Figure 5. SF-Abs kinetics of the reaction of 100 μM Fe(III)-SDO and 3NG with $O_2^{\bullet-}$. (A) Diode array spectra recorded between 0.018 – 10 s. (B) Change in the absorbance during the course of the reaction.

Discussion

Reaction cycles of non-heme iron dioxygenases are believed to be initiated upon binding of dioxygen to the ferrous center from partial transfer of the electron density from Fe center to the dioxygen moiety, yielding a formally Fe(III)-superoxo moiety. Homoprotocatechuate 2,3-dioxygenase (HPCD) is a ring cleaving dioxygenase whose reaction cycle has been extensively characterized, including a spectroscopically and structurally characterized Fe(III)-superoxo intermediate.[18, 31] The iron cofactors in HPCD and SDO afford aromatic ring cleavage and dioxygenase activity (Scheme S1), while bearing striking similarities and differences in the active sites. An overlay of the two active sites is shown in Figure 6. The Fe cofactor in SDO is tethered to a relatively rare 3-His motif, in contrast to the common 2-His-1-Carboxylate coordination sphere of HPCD. HPCD contains a histidine residue (H200) placed in the vicinity of the bound dioxygen, which plays a critical role in the enzymatic cycle and acts as a proton acceptor during catalysis. In the active site of SDO, an arginine residue (Arg127) is found at a similar location and expected to interact with O_2 or the substrate upon their binding. However, recent studies on a related ring-cleaving 5-nitrosalicylate 1,2-dioxygenase suggest that arginine may not be necessary for dioxygenase activity of cupin dioxygenases.[36] Furthermore, QM studies have suggested that contrary to HPCD, O_2 activation in SDO does not require a proton source.[16] The data presented here allows us to evaluate the influence of these differences in the primary and the secondary coordination spheres in the context of thermodynamics and kinetics of the reaction profile, particularly O_2 binding.

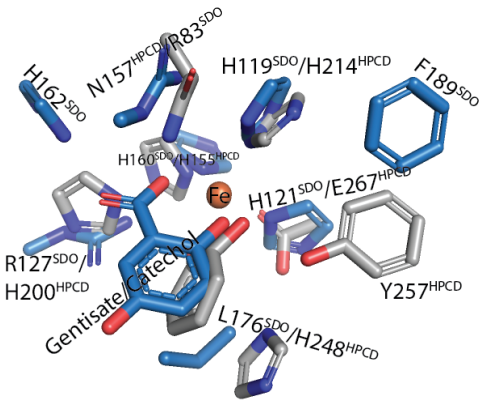

Figure 6. Overlay of the active sites of substrate bound SDO (blue, PDB: 3NL1) and HPCD (gray, PDB: 2IGA). Backbone and several sidechain atoms have been removed for clarity.

The oxy complex formed during H200N HPCD catalyzed reaction consists of superoxide radical coupled to iron center in a high-spin ferric state, yielding a Fe(III)-superoxo intermediate which exhibits a

λ_{max} of 506 nm, while the corresponding ES complex of the enzyme absorbs at 518 nm.[18] Biomimetic complexes catalyzing reactions of catechols and O_2 to yield extradiol products also form oxygen intermediates with absorption maxima between 535 to 600 nm.[37] Similarly, other synthetic Fe(III)-superoxo complexes mimicking mononuclear ferric superoxo intermediates also exhibit optical chromophore between 500-600 nm.[38-40] The optical feature of Fe(III)-SDO-3NG-$O_2^{\bullet-}$ complex at 495 nm is clearly distinct from the optical spectrum of I1.

Our kinetic study shows that formation of I1 can be described using a second order rate constant, with the RRT of the corresponding phase of the reaction directly dependent on the dissolved O_2 concentration. Based on this observation, we propose that I1 may represent the oxy adduct of SDO. While additional data is needed to fully characterize I1, below we discuss the electronic nature of I1 as a putative oxy adduct of SDO. The electronic structure of I1 is not equivalent to the in situ generated Fe(III)-SDO-3NG-$O_2^{\bullet-}$ complex, indicating that the electronic structure of I1 does not correspond to an Fe(III)-superoxo species. Alternatively, I1 can be described as Fe(II)-O_2 complex, wherein the electronic spin of the Fe center remains in the quintet state and the aromaticity of the nitrogentisate ring is still intact in accordance with the small blue shift in the chromophore of I1 compared with the bound substrate. This proposal is supported by previous quantum mechanical (QM) calculation on salicylate-Fe(II)-O_2 complex of SDO.[16] Out of seven resonance structures including an Fe(III)-superoxo electronic configuration, salicylate-Fe(II)-O_2 complex was found to be best described as an Fe(II)-O_2 or Fe(II)-$O_2^{\bullet-}$ center with partial electron density transfer from the substrate leading to its activation. Lack of an optical chromophore near 500-600 nm range for I1 in the SF-Abs kinetics studies reported here provides experimental evidence for the QM calculations. We note that in another QM study, the electronic structure of SDO oxy adduct was assigned as an Fe(III)-$O_2^{\bullet-}$ species.[41] The authors attributed this discrepancy to differences in the size of the active sites models in the two studies. The oxy adduct of SDO could also represent a Fe(II)-$O_2^{\bullet-}$ species bound to a semiquinone radical. Such a species can be formed once the substrate donates an electron to the transient Fe(III)-$O_2^{\bullet-}$ complex. However, the aromaticity of the substrate will not be preserved in this putative [semiquinone radical]-Fe(II)-$O_2^{\bullet-}$ intermediate. To summarize, while both SDO and HPCD perform ring scission of their aromatic substrates, our data suggests that their oxy adduct have different electronic properties indicating that oxygen activation in the two enzymes may take place via different mechanisms.

The proposed reaction mechanism of SDO (Scheme 2) entails formation of an alkylperoxo intermediate upon the transfer of an electron from the substrate to the metal center. A similar intermediate has been detected and spectroscopically characterized in the reaction cycle of H200N variant of HPCD.[18, 29] Depending on the substrate, the rate of formation of this intermediate varied between 0.02 – 0.5 s^{-1}. The rate of accumulation of I2 in the reaction of SDO reported here (k_2 =1.3 s^{-1}) is similar to that of the

alkylperoxo intermediate in HPCD. Therefore, based on these observed rates and the proposed reaction mechanism of SDO, we suggest that I2 may represent an alkylperoxo intermediate.

Influence of the primary and secondary coordination sphere on dioxygen binding rates: Insights from density functional theory calculations. Extensive work by Lipscomb and co-workers have demonstrated that secondary sphere interactions modulate the kinetics for dioxygen binding. Rates of O_2 binding ($k_{on}^{O_2}$) for four variants of HPCD generated by mutating residue H200 that servers as an acid/base during catalysis showed up to six-fold variations.[42] We note that the k_{on}^{O2} for the wild type HPCD was too fast to be quantified. While these variations are significant, O_2 binding to the ferrous center in SDO (k_1 = 5.9 x 10^3 $M^{-1}s^{-1}$) takes place at a rate two orders of magnitude slower compared to HPCD mutants catalyzing the conversion of similar nitro-substrate ($k_{on}^{O_2}$ for the nitrocatechol reaction of H200N HPCD = 1.5 x 10^5 $M^{-1}s^{-1}$).[29] The secondary coordination spheres of SDO and HPCD bear several similarities and differences (Figure S5). As demonstrated for HPCD, while modifications in the secondary coordination sphere can influence $k_{on}^{O_2}$, it is unlikely that these variations are solely responsible for the large differences in $k_{on}^{O_2}$ between the two enzymes. Alternatively, the differences in the primary coordination sphere of the two enzymes may render a greater influence.

The substitution of a carboxylate ligand in HPCD with a histidine residue in SDO increases the charge of the metal-protein derived ligand complex by +1. Furthermore, imidazole is a stronger field ligand compared to the carboxylate moiety and the ground state electronic properties of the metal cofactor are expected to vary in the two motifs. Differences in the net charge of the metal-ligand complex are expected to affect the local electrostatic potential of the metal-ligand cluster. To quantify this influence of the charge of the primary coordination sphere, we employed density functional theory (DFT) calculations. The calculated electrostatic potential of a 3-His-Fe-3NG metal-ligand cluster was ca. 1.5 eV lower than that of a 2-His-1-Carboxylate-Fe-3NG cluster. This significant difference in the local electrostatic potential underscores the impact of the net charge of primary coordination sphere on modulating the electron donor ability of the iron cofactor and therefore its electronic structure. With an elevated local electrostatic potential, a 2-His-1-Carboxylate bound ferrous center would have a greater propensity to donate its electron to the O_2 π^* orbitals and formally achieve an Fe(III)-$O_2^{\bullet-}$ electronic structure. Conversely, a more positive 3-His binding motif hinders electron donation owing to its suppressed electrostatic potential.

Spin population of the metal center is usually used as a gauge to predict its oxidation state in DFT calculations and the choice and the size of the cluster has been shown to influence the calculated spin populations.[18-19, 41] Indeed, irrespective of the primary and secondary sphere environment, the oxy adduct is expected to entail transfer of some electron density from the metal cofactor to the bound dioxygen. The data presented here suggests that the primary coordination sphere, by the virtue of its net charge, can

modulate the extent of the electron transfer and consequently has significant impact on the electronic structure of the reaction intermediates. A 3-His motif hinders the transfer of electron from the metal cofactor and therefore may support an oxy adduct with iron cofactor bearing electron density closer to the quintet state of its precursor. In light of these results, it is plausible that the dramatic differences in $k_{on}^{O_2}$ of the two enzymes originates from the differences in the net charge of their primary coordination spheres.

While the differences in $k_{on}^{O_2}$ for the two enzymes is striking, they translate to relatively small changes in the free energy of dioxygen binding (ΔG^{SDO} = -4.5 kcal/mol vs. ΔG^{HPCD} = -4.7 kcal/mol). Presumably, variations in enzymatic active sites render greater influence on the kinetics of catalysis while leaving the thermodynamics relatively unchanged. Indeed, from the perspective of overall catalysis, the two enzymes perform energetically similar transformations with comparable efficiency. Enzymatic active sites may balance the thermodynamics of O_2 activation by modulating the electronic properties of their oxy-adducts.

Conclusions

Oxygen activation in aromatic ring cleaving dioxygenases has been proposed to take place via the formation of oxy adducts. We employed transient kinetic measurements to monitor the reaction cycle of SDO using an analog to its natural substrate. The results suggest that the first intermediate, I1, formed at a forward rate of 5.9 x 10^3 $M^{-1}s^{-1}$ and the electronic structure of this intermediate is not consistent with an Fe(III)-superoxo moiety. DFT calculations suggest that the primary coordination sphere of SDO may hinder the transfer of electron density to bound dioxygen in SDO. Collectively, the results reported herein suggest that the O_2 activation in SDO may take place via a pathway different from the generally accepted mechanism of extradiol ring dioxygenases. Given that various non-heme enzymes with distinct metal primary spheres execute similar chemical transformations, it is appealing to argue if the active site tuning in enzymes can alter the electronic properties of the reaction intermediates. However, the influence of these changes should be evaluated in the context of both the thermodynamics and kinetics of the reaction coordinates. Such consideration may help understand the origin of biological deviation in active sites and provide additional principals for design of artificial enzymes.

Experimental Methods

***Protein expression and purification*.** SDO cDNA sequence containing a TEV cleavage site (ENLYFQG) was synthesized (GenScript) and cloned into a pET-41a+ plasmid leaving a His-tag at the N-terminal of SDO open reading frame. The plasmid was transformed into *E.coli* BL21(DE3) strain for overexpression. Cell culture was grown in Luria Broth medium at 37 °C until OD_{600} reached 0.6. After lowering the temperature to 20 °C, ferrous ammonium sulfate and 0.1 mM isopropyl β-d-1-thiogalactopyranoside were added. Cells were harvested after 15 hours of induction by centrifugation at 8,000 rpm and 4 °C. The cell

pellet was resuspended in lysis buffer (Tris 50 mM, sodium chloride 300 mM, imidazole 5 mM, pH 8.0) and sonicated followed by centrifugation at 16,000 rpm for 40 min at 4 °C. The supernatant was loaded onto a HisTrap column equilibrated with binding buffer (Tris 50 mM, sodium chloride 100 mM, imidazole 5 mM, pH 8.0) and the protein was eluted with a gradient of elution buffer (Tris 50 mM, sodium chloride 100 mM, imidazole 800 mM, pH 8.0). Imidazole was removed by passing the sample through a HiTrap desalting column leading to the final working buffer (Tris 20 mM, sodium chloride 100 mM, pH 8.0). The purity and yield were established using SDS-PAGE gel and absorbance at 280 nm assuming a molar extinction coefficient of 74.0 mM^{-1} cm^{-1}. To remove the His-tag, the protein was incubated with His-tag labeled TEV protease followed by separation using an additional HisTrap chromatography step. Iron incorporation in the purified protein was estimated by spectrophotometric methods following previously published protocols.[43-44] Typically, iron occupancy of 70-80 % iron was observed for all batches of the purified protein. The Mössbauer spectrum of ^{57}Fe enriched SDO is presented in Figure S5. The isomer shift and quadrupolar splitting is indicative of a high-spin ferrous species with no evidence of speciation and negligible ferric impurities. The observed Mössbauer parameters are different from that of free ferrous in the same buffer conditions (data not shown). These results indicate that quantitatively, majority of Fe incorporated in the protein is in catalytically active ferrous state. Based on these findings, concentration of iron determined from the spectrophotometric assay was considered as the concentration of active enzyme. To account for variations in the iron occupancy, Fe concentration was determined separately for each batch of protein upon purification.

Synthesis and characterization of 3-nitrogentisic acid (3NG). The synthesis of 3NG was accomplished based on the reaction shown below using the following procedure. The starting material, 3-nitrosalicylic acid (3NS), was obtained from TCI Chemicals. In a suitable reaction vessel, 0.5 g of 3NS was dissolved in 10 mL of 2 M sodium hydroxide (NaOH) solution, followed by the addition of 20 mL of a 27.5 g/L potassium persulfate stock solution. The reaction mixture was stirred at room temperature for 2 days. Subsequently, the solution was acidified with diluted sulfuric acid on ice until a yellow precipitate was formed. Unreacted 3NS and precipitated impurities were extracted using diethyl ether in a separatory funnel. The extraction process was repeated at least 3 times. The resulting aqueous layer was strongly acidified with diluted sulfuric acid and boiled for 30 minutes. After cooling to room temperature and further chilling on ice for 10 minutes, brown crystals were obtained. The crystals were isolated by vacuum filtration and optionally subjected to recrystallization for additional purification. The identity and purity of the product were confirmed by LC-MS and solution ^{1}H- and ^{13}C-NMR analyses. Figure S6 shows ^{1}H NMR spectrum of 3NG in D_2O acquired at 14.1 T with the following resonances, δ (ppm): 7.73 (d, J = 2.6 Hz, 1H, 6-H), 7.69 ppm (d, J = 2.8 Hz, 1H, 4-H). ^{13}C NMR spectrum of the synthesized compound in DMSO-

d_6 presented in Figure S7 exhibited δ (ppm) at: 170.7, 148.2, 148.0, 137.8, 122.0, 117.0, 116.8. Both ^{1}H- and ^{13}C-NMR are consistent with the expected molecular structure of 3NG. High resolution mass spectrometry (ESI) showed a major signal at 198.0055 $[M-H]^-$, consistent with calculated m/z for 3NG ($C_7H_4NO_6$) at 198.0044.

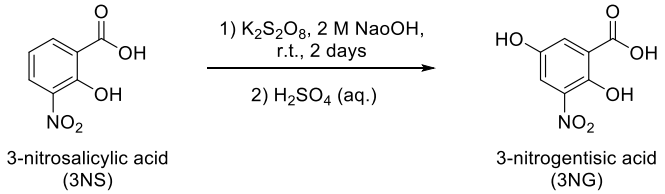

Steady state kinetic measurements. Michaelis-Menten parameters were determined by monitoring the rate of product formation or substrate degradation using Shimadzu UV-2700 spectrometer equipped with Quantum Northwest TC 1 temperature controller. Enzyme activity was measured at 22 or 4 ºC in 50 mM Tris, 100 mM NaCl buffer prepared at pH 8.0. Rate of product (maleylpyruvate) formation for the reaction of SDO with gentisate was monitored at 380 nm (ε_{380} = 2.4 $mM^{-1}cm^{-1}$). The rate of substrate consumption for the reaction of 3NG with SDO was monitored at 510 nm (ε_{510} = 0.32 $mM^{-1}cm^{-1}$). Typically, the substrate concentration was varied between 0.05 to 2 mM. A hyperbolic fit to the initial velocity data generated as a function of substrate concentration was used to determine the K_m and V_{max} values.

Anaerobic manipulations and oxygen concentration measurements. Anerobic solutions of 3NG were prepared by degassing on a Schlenk line. Anaerobic enzyme samples were prepared by gently purging argon gas while maintaining the enzyme solution at 4 ºC. Degassed enzyme and substrate solution were anaerobically mixed on the Schlenk line before transferring to the stopped flow device. In preparation for the stopped-flow experiments, a series of dissolved oxygen buffers with varying oxygen concentrations were prepared. Two stock solutions were used. The first stock solution was purged with ambient air at 4 ºC for 20 minutes (buffer A), while the second stock solution was purged with pure oxygen gas for the same duration and at the same temperature (buffer B). The two stock solutions were then combined in different proportions, specifically 0%, 20%, 40%, 60%, 80%, and 100% of buffer B. Final oxygen concentration for each buffer was verified with a Clark type electrode (Oxytherm+ manufactured by Hansatech Instruments, Norfolk, England) by employing the standard operating protocols provided by the manufacturer at 4 ºC. This approach ensured the generation of buffers with precise and controlled dissolved oxygen levels for the stopped-flow experiments.

Transient kinetic experiments. All transient kinetics experiments were performed using Applied Photophysics SX20 stopped-flow device. For the reaction of Fe(II)-SDO-3NG with O_2, anaerobic ES

complex was rapidly mixed with oxygenated buffer prepared at various concentrations ranging between 0.3 and 1.8 mM at 4 ºC. The binding affinity of 3NG and SDO is not known. Therefore, to maintain single turnover conditions excess enzyme and limiting amounts of substrate were used assuming an upper limit of $K_d \sim K_m$ (2 mM SDO mixed with 200 μM 3NG to generate ~ 100 μM Fe(II)-3NG-SDO complex). Kinetic data was collected using a diode array detector with time increments of 1 ms. The observed absorbance ($A_{t,obs}$) during the time course of the reaction at a single wavelength was fitted to sums of exponential functions: $A_{t,obs} = \sum_{i=0}^{n} A_i e^{(-\frac{t}{\tau_i})} + A_\infty$, where the observed amplitude in absorbance units for phase i (out of n) is given by A_i; the reciprocal relaxation time for the same phase is given by $1/\tau_i$; time is denoted by t (in seconds) and A_∞ represent the absorbance at the end of the reaction. Nonlinear regression fitting of the data yielded reciprocal relaxation times (RRT) and amplitudes of different phases of the reaction. The RRTs were determined by global fitting of 10 different wavelengths between 340 and 700 nm. A single exponential corresponding to a $1/\tau$ of 0.025 s^{-1} corresponding to non-enzymatic product degradation (Figure S8) was subtracted from all wavelengths analyzed. For the reaction of Fe(III)-SDO-3NG with superoxide anion, the ferric enzyme complex was aerobically prepared and rapidly mixed with superoxide anions generated by xanthine oxidase in the presence of xanthine.

Preparation of oxidized enzyme. Our attempts to oxidize the iron cofactor with several common oxidants were unsuccessful due to protein denaturation upon treatment. In another independent study, we identified catechols as competitive inhibitors of gentisate (unpublished results). However, unlike unsubstituted catechol, we noticed loss in enzyme activity upon treatment with 4-nitrocatechol (4NC). Electron paramagnetic studies demonstrated that treatment with 4NC quantitatively converted the ferrous cofactor to ferric suggesting that 4NC can oxide the enzyme. The mechanism of 4NC oxidation of SDO is currently under investigation and will be a focus of a separate study. To generate the oxidized enzyme, 100 μM SDO was treated with 5 mM 4NC and incubated at 4 ºC for 15 hours. Subsequently, the solution was loaded onto a HiTrap desalting column, which allowed for the separation of SDO protein from excess 4NC and reaction products. EPR spectrum for Fe(II)-SDO treated with 4NC is shown in Figure S9. Prior to the addition of 4NC, no ferric species is detected in the sample, consistent with the Mössbauer results reported in Figure S5. After treatment with 4NC (as described above), an isotropic signal at g=4.3 is observed. This transition is indicative of high spin ferric complex, which is in quantitative agreement with the expected starting Fe(II)-SDO concentration. Additionally, the oxidized enzyme was concentrated using a 50 kDa cutoff centricon device and the flow through was collected. The iron content of the flow through was spectrophotometrically determined. In this test we found negligible amounts of Fe in the buffer suggesting that the oxidized enzyme does not contain free Fe.

Generation of superoxide from xanthine oxidase. Enzymatic generation of superoxide anions was achieved by xanthine oxidase (XO). In a typical experiment, superoxide anion generation was initiated by addition of 0.4 units of XO to O_2 or air purged buffer containing 6 mM xanthine prepared at a pH of 8.2. Quantitation of accumulated superoxide anions was performed by monitoring the reduction of cytochrome c at 550 nm using $\Delta\varepsilon = 21000\ M^{-1}\ cm^{-1}$ as previously reported.[33]

Density functional theory calculations. The 3-His model cluster was constructed based on the crystal structure of salicylate bound SDO (PDB: 3NJZ).[13] Briefly, we extracted the coordinates of the metal cofactor, the 3 metal binding histidines (His119, His121, and His160), the substrate, and the neighboring arginine (Arg127). The amino acids were truncated at the Cα atoms and saturated with hydrogen, salicylate was modified to 3NG, and O_2 was added to the metal cofactor. A net charge of +1 was assigned to this cluster. To construct the 2-His-1-Carboxylate model cluster, the crystal structure of salicylate bound SDO was overlaid with the crystal structure of substrate bound homoprotocatechuate 2,3-dioxygenase (PDB: 2IGA)[31] and the coordinates of His121 in the SDO crystal structure were replaced by Glu267 from the latter crystal structure. The 2-His-1-Carboxylate model cluster was truncated and completed as the 3-His model cluster. A net charge of 0 was assigned to this cluster. Density functional theory (DFT) calculations were carried out with ORCA 5.0.[45] Geometries were optimized at the B3LYP[46-47]/ def2-TZVP[48-49] level in the gas phase by constraining the positions of selected peripherical atoms; the geometries of the optimized clusters showing the constrained atoms are shown in Figure S10. To estimate the local electrostatic potential, we calculated the ionization potentials of the metal-ligand units. Single-point energy calculations were carried out by employing the optimized 3-His and 2-His-1-Carboxylate model clusters, devoid of the O_2 molecule and Arg127. Additional details of DFT calculations and results are provided in the Supplementary Information.

Acknowledgements

This work was supported by the National Science Foundation Grants CHE-2107692 and OAC-2215760. We thank Professor David Lacy at the University of Buffalo for insightful discussions.

References

(1) Vaillancourt, F. H.; Bolin, J. T.; Eltis, L. D. The ins and outs of ring-cleaving dioxygenases. *Crit Rev Biochem Mol Biol* **2006**, *41* (4), 241-267. DOI: 10.1080/10409230600817422
(2) Harpel, M. R.; Lipscomb, J. D. Gentisate 1,2-dioxygenase from Pseudomonas acidovorans. *Methods Enzymol.* **1990**, *188*, 101-107. DOI: 10.1016/0076-6879(90)88019-7

(3) Harpel, M. R.; Lipscomb, J. D. Gentisate 1,2-dioxygenase from Pseudomonas. Substrate coordination to active site Fe^{2+} and mechanism of turnover. *J. Biol. Chem.* **1990**, *265* (36), 22187-22196.
(4) Harpel, M. R.; Lipscomb, J. D. Gentisate 1,2-dioxygenase from pseudomonas. Purification, characterization, and comparison of the enzymes from Pseudomonas testosteroni and Pseudomonas acidovorans. *J. Biol. Chem.* **1990**, *265* (11), 6301-6311.
(5) Dunwell, J. M.; Purvis, A.; Khuri, S. Cupins: the most functionally diverse protein superfamily? *Phytochemistry* **2004**, *65* (1), 7-17. DOI: https://doi.org/10.1016/j.phytochem.2003.08.016
(6) Hintner, J.-P.; Lechner, C.; Riegert, U.; Kuhm, A. E.; Storm, T.; Reemtsma, T.; Stolz, A. Direct Ring Fission of Salicylate by a Salicylate 1,2-Dioxygenase Activity from Pseudaminobacter salicylatoxidans. *Journal of Bacteriology* **2001**, *183* (23), 6936-6942. DOI: 10.1128/jb.183.23.6936-6942.2001
(7) Ferraroni, M.; Matera, I.; Bürger, S.; Reichert, S.; Steimer, L.; Scozzafava, A.; Stolz, A.; Briganti, F. The salicylate 1,2-dioxygenase as a model for a conventional gentisate 1,2-dioxygenase: crystal structures of the G106A mutant and its adducts with gentisate and salicylate. *The FEBS Journal* **2013**, *280* (7), 1643-1652. DOI: 10.1111/febs.12173
(8) Hintner, J.-P.; Reemtsma, T.; Stolz, A. Biochemical and Molecular Characterization of a Ring Fission Dioxygenase with the Ability to Oxidize (Substituted) Salicylate(s) from Pseudaminobacter salicylatoxidans. *J. Biol. Chem.* **2004**, *279* (36), 37250-37260. DOI: 10.1074/jbc.M313500200
(9) Matera, I.; Ferraroni, M.; Burger, S.; Scozzafava, A.; Stolz, A.; Briganti, F. Salicylate 1,2-dioxygenase from Pseudaminobacter salicylatoxidans: crystal structure of a peculiar ring-cleaving dioxygenase. *J. Mol. Biol.* **2008**, *380* (5), 856-868. DOI: 10.1016/j.jmb.2008.05.041
(10) Eppinger, E.; Bürger, S.; Stolz, A. Spontaneous release of fluoride during the dioxygenolytic cleavage of 5-fluorosalicylate by the salicylate 1,2-dioxygenase from Pseudaminobacter salicylatoxidans BN12. *FEMS Microbiol. Lett.* **2015**, *363* (1). DOI: 10.1093/femsle/fnv211
(11) Sánchez-Arroyo, A.; Plaza-Vinuesa, L.; Rivas, B. d. l.; Mancheño, J. M.; Muñoz, R. The salicylate 1,2-dioxygenase from Pseudaminobacter salicylatoxidans DSM 6986T is a bifunctional enzyme that inactivates the mycotoxin ochratoxin A by a novel amidohydrolase activity. *Int. J. Biol. Macromol.* **2023**, *237*, 124230. DOI: https://doi.org/10.1016/j.ijbiomac.2023.124230
(12) Ferraroni, M.; Steimer, L.; Matera, I.; Burger, S.; Scozzafava, A.; Stolz, A.; Briganti, F. The generation of a 1-hydroxy-2-naphthoate 1,2-dioxygenase by single point mutations of salicylate 1,2-dioxygenase--rational design of mutants and the crystal structures of the A85H and W104Y variants. *J. Struct. Biol.* **2012**, *180* (3), 563-571. DOI: 10.1016/j.jsb.2012.08.007
(13) Ferraroni, M.; Matera, I.; Steimer, L.; Burger, S.; Scozzafava, A.; Stolz, A.; Briganti, F. Crystal structures of salicylate 1,2-dioxygenase-substrates adducts: A step towards the comprehension of the structural basis for substrate selection in class III ring cleaving dioxygenases. *J. Struct. Biol.* **2012**, *177* (2), 431-438. DOI: 10.1016/j.jsb.2011.11.026
(14) Aleshintsev, A.; Eppinger, E.; Groning, J. A. D.; Stolz, A.; Gupta, R. Substrate promiscuity and active site differences in gentisate 1,2-dioxygenases: electron paramagnetic resonance study. *J. Biol. Inorg. Chem.* **2019**, *24* (2), 287-296. DOI: 10.1007/s00775-019-01646-5
(15) Eppinger, E.; Ferraroni, M.; Burger, S.; Steimer, L.; Peng, G.; Briganti, F.; Stolz, A. Function of different amino acid residues in the reaction mechanism of gentisate 1,2-dioxygenases deduced from the analysis of mutants of the salicylate 1,2-dioxygenase from Pseudaminobacter salicylatoxidans. *Biochim. Biophys. Acta* **2015**, *1854* (10 Pt A), 1425-1437. DOI: 10.1016/j.bbapap.2015.06.005
(16) Roy, S.; Kästner, J. Synergistic Substrate and Oxygen Activation in Salicylate Dioxygenase Revealed by QM/MM Simulations. *Angew. Chem., Int. Ed.* **2016**, *55* (3), 1168-1172. DOI: 10.1002/anie.201506363
(17) Wang, Y.; Li, J.; Liu, A. Oxygen activation by mononuclear nonheme iron dioxygenases involved in the degradation of aromatics. *J. Biol. Inorg. Chem.* **2017**, *22* (2-3), 395-405. DOI: 10.1007/s00775-017-1436-5
(18) Mbughuni, M. M.; Chakrabarti, M.; Hayden, J. A.; Bominaar, E. L.; Hendrich, M. P.; Munck, E.; Lipscomb, J. D. Trapping and spectroscopic characterization of an Fe-III-superoxo intermediate from a nonheme mononuclear iron-containing enzyme. *Proc. Natl. Acad. Sci. U. S. A.* **2010**, *107* (39), 16788-16793. DOI: 10.1073/pnas.1010015107

(19) Christian, G. J.; Ye, S.; Neese, F. Oxygen activation in extradiol catecholate dioxygenases – a density functional study. *Chem. Sci.* **2012**, *3* (5), 1600-1611, 10.1039/C2SC00754A. DOI: 10.1039/C2SC00754A
(20) Tamanaha, E.; Zhang, B.; Guo, Y.; Chang, W.-c.; Barr, E. W.; Xing, G.; St. Clair, J.; Ye, S.; Neese, F.; Bollinger, J. M., Jr.; et al. Spectroscopic Evidence for the Two C–H-Cleaving Intermediates of Aspergillus nidulans Isopenicillin N Synthase. *J. Am. Chem. Soc.* **2016**, *138* (28), 8862-8874. DOI: 10.1021/jacs.6b04065
(21) Crawford, J. A.; Li, W.; Pierce, B. S. Single Turnover of Substrate-Bound Ferric Cysteine Dioxygenase with Superoxide Anion: Enzymatic Reactivation, Product Formation, and a Transient Intermediate. *Biochemistry* **2011**, *50* (47), 10241-10253. DOI: 10.1021/bi2011724
(22) Roy, S.; Kästner, J. Catalytic Mechanism of Salicylate Dioxygenase: QM/MM Simulations Reveal the Origin of Unexpected Regioselectivity of the Ring Cleavage. *Chem. – Eur. J.* **2017**, *23* (37), 8949-8962. DOI: 10.1002/chem.201701286
(23) Koehntop, K. D.; Emerson, J. P.; Que, L., Jr. The 2-His-1-carboxylate facial triad: a versatile platform for dioxygen activation by mononuclear non-heme iron(II) enzymes. *J. Biol. Inorg. Chem.* **2005**, *10* (2), 87-93. DOI: 10.1007/s00775-005-0624-x
(24) Kal, S.; Que, L. Dioxygen activation by nonheme iron enzymes with the 2-His-1-carboxylate facial triad that generate high-valent oxoiron oxidants. *J. Biol. Inorg. Chem.* **2017**, *22* (2-3), 339-365. DOI: 10.1007/s00775-016-1431-2
(25) Traore, E. S.; Liu, A. Charge Maintenance during Catalysis in Nonheme Iron Oxygenases. *ACS Catal.* **2022**, *12* (10), 6191-6208. DOI: 10.1021/acscatal.1c04770
(26) Lipscomb, J. D.; Orville, A. M. Mechanistic Aspects of Dihydroxybenzoate Dioxygenases. In *Metal ions in Biological Systems*, Sigel, A., Sigel, H. Eds.; Vol. 28; CRC press, 1992.
(27) Gopal, B.; Madan, L. L.; Betz, S. F.; Kossiakoff, A. A. The Crystal Structure of a Quercetin 2,3-Dioxygenase from Bacillus subtilis Suggests Modulation of Enzyme Activity by a Change in the Metal Ion at the Active Site(s). *Biochemistry* **2005**, *44* (1), 193-201. DOI: 10.1021/bi0484421
(28) Kloer, D. P.; Ruch, S.; Al-Babili, S.; Beyer, P.; Schulz, G. E. The Structure of a Retinal-Forming Carotenoid Oxygenase. *Science* **2005**, *308* (5719), 267. DOI: 10.1126/science.1108965
(29) Groce, S. L.; Lipscomb, J. D. Aromatic ring cleavage by homoprotocatechuate 2,3-dioxygenase: Role of His200 in the kinetics of interconversion of reaction cycle intermediates. *Biochemistry* **2005**, *44* (19), 7175-7188. DOI: 10.1021/bi050180v
(30) Groce, S. L.; Miller-Rodeberg, M. A.; Lipscomb, J. D. Single-turnover kinetics of homoprotocatechuate 2,3-dioxygenase. *Biochemistry* **2004**, *43* (48), 15141-15153. DOI: 10.1021/bi048690x
(31) Kovaleva, E. G.; Lipscomb, J. D. Crystal Structures of Fe^{2+} Dioxygenase Superoxo, Alkylperoxo, and Bound Product Intermediates. *Science* **2007**, *316* (5823), 453-457. DOI: doi:10.1126/science.1134697
(32) Knoot, C. J.; Purpero, V. M.; Lipscomb, J. D. Crystal structures of alkylperoxo and anhydride intermediates in an intradiol ring-cleaving dioxygenase. *Proc. Natl. Acad. Sci. U. S. A.* **2015**, *112* (2), 388-393. DOI: doi:10.1073/pnas.1419118112
(33) Fridovich, I. Quantitative aspects of the production of superoxide anion radical by milk xanthine oxidase. *J. Biol. Chem.* **1970**, *245* (16), 4053-4057.
(34) McCord, J. M.; Fridovich, I. The reduction of cytochrome c by milk xanthine oxidase. *J. Biol. Chem.* **1968**, *243* (21), 5753-5760.
(35) Crack, J. C.; Green, J.; Cheesman, M. R.; Le Brun, N. E.; Thomson, A. J. Superoxide-mediated amplification of the oxygen-induced switch from [4Fe-4S] to [2Fe-2S] clusters in the transcriptional regulator FNR. *Proc. Natl. Acad. Sci. U. S. A.* **2007**, *104* (7), 2092-2097. DOI: doi:10.1073/pnas.0609514104
(36) Eppinger, E.; Stolz, A.; Ferraroni, M. Crystal structure of the monocupin ring-cleaving dioxygenase 5-nitrosalicylate 1,2-dioxygenase from Bradyrhizobium sp. *Acta Crystallographica Section D* **2023**, *79* (7). DOI: doi:10.1107/S2059798323004199

(37) Jo, D.-H.; Chiou, Y.-M.; Que, L. Models for Extradiol Cleaving Catechol Dioxygenases: Syntheses, Structures, and Reactivities of Iron(II)−Monoanionic Catecholate Complexes. *Inorg. Chem.* **2001**, *40* (13), 3181-3190. DOI: 10.1021/ic001185d
(38) Chiang, C.-W.; Kleespies, S. T.; Stout, H. D.; Meier, K. K.; Li, P.-Y.; Bominaar, E. L.; Que, L., Jr.; Münck, E.; Lee, W.-Z. Characterization of a Paramagnetic Mononuclear Nonheme Iron-Superoxo Complex. *J. Am. Chem. Soc.* **2014**, *136* (31), 10846-10849. DOI: 10.1021/ja504410s
(39) Hong, S.; Sutherlin, K. D.; Park, J.; Kwon, E.; Siegler, M. A.; Solomon, E. I.; Nam, W. Crystallographic and spectroscopic characterization and reactivities of a mononuclear non-haem iron(III)-superoxo complex. *Nat. Commun.* **2014**, *5* (1), 5440. DOI: 10.1038/ncomms6440
(40) Oddon, F.; Chiba, Y.; Nakazawa, J.; Ohta, T.; Ogura, T.; Hikichi, S. Characterization of Mononuclear Non-heme Iron(III)-Superoxo Complex with a Five-Azole Ligand Set. *Angew. Chem., Int. Ed.* **2015**, *54* (25), 7336-7339. DOI: https://doi.org/10.1002/anie.201502367
(41) Dong, G.; Ryde, U. O2 Activation in Salicylate 1,2-Dioxygenase: A QM/MM Study Reveals the Role of His162. *Inorg. Chem.* **2016**, *55* (22), 11727-11735. DOI: 10.1021/acs.inorgchem.6b01732
(42) Mbughuni, M. M.; Chakrabarti, M.; Hayden, J. A.; Meier, K. K.; Dalluge, J. J.; Hendrich, M. P.; Münck, E.; Lipscomb, J. D. Oxy Intermediates of Homoprotocatechuate 2,3-Dioxygenase: Facile Electron Transfer between Substrates. *Biochemistry* **2011**, *50* (47), 10262-10274. DOI: 10.1021/bi201436n
(43) Pierce, B. S.; Gardner, J. D.; Bailey, L. J.; Brunold, T. C.; Fox, B. G. Characterization of the Nitrosyl Adduct of Substrate-Bound Mouse Cysteine Dioxygenase by Electron Paramagnetic Resonance: Electronic Structure of the Active Site and Mechanistic Implications. *Biochemistry* **2007**, *46* (29), 8569-8578. DOI: 10.1021/bi700662d
(44) Collins, P. F.; Diehl, H.; Smith, G. F. 2,4,6-Tripyridyl-s-triazine as Reagent for Iron. Determination of Iron in Limestone, Silicates, and Refractories. *Anal. Chem.* **1959**, *31* (11), 1862-1867. DOI: 10.1021/ac60155a056
(45) Neese, F. Software update: The ORCA program system—Version 5.0. *WIREs Computational Molecular Science* **2022**, *12* (5), e1606. DOI: https://doi.org/10.1002/wcms.1606
(46) Becke, A. D. Density-functional thermochemistry. III. The role of exact exchange. *J. Chem. Phys.* **1993**, *98* (7), 5648-5652. DOI: 10.1063/1.464913
(47) Lee, C.; Yang, W.; Parr, R. G. Development of the Colle-Salvetti correlation-energy formula into a functional of the electron density. *Phys. Rev. B* **1988**, *37* (2), 785-789. DOI: 10.1103/PhysRevB.37.785
(48) Weigend, F.; Ahlrichs, R. Balanced basis sets of split valence, triple zeta valence and quadruple zeta valence quality for H to Rn: Design and assessment of accuracy. *Phys. Chem. Chem. Phys.* **2005**, *7* (18), 3297-3305, 10.1039/B508541A. DOI: 10.1039/B508541A
(49) Weigend, F. Accurate Coulomb-fitting basis sets for H to Rn. *Phys. Chem. Chem. Phys.* **2006**, *8* (9), 1057-1065, 10.1039/B515623H. DOI: 10.1039/B515623H

TOC graphics:

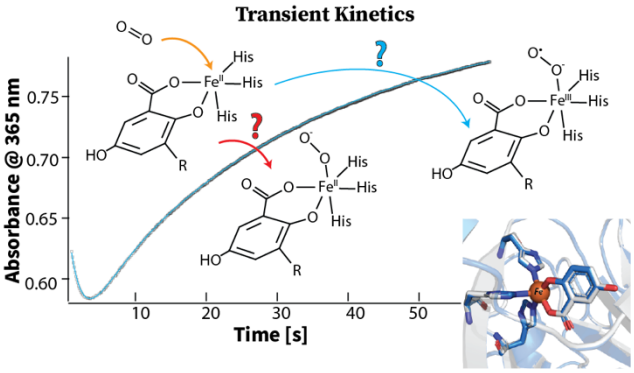

TOC text:

Salicylate dioxygenase performs aromatic C-C bond scission of its substrates, salicylate and gentisate, with the aid of iron cofactor tethered to a 3-His binding motif. By utilizing a nitro substituted substrate analog, which attenuates the enzymatic k_{cat} by 500-fold, detection and kinetics characterization two reaction intermediates was performed with stopped-flow optical absorption spectroscopy.